

RESEARCH ARTICLE SUMMARY

MICROBIOTA

Endocytosis of commensal antigens by intestinal epithelial cells regulates mucosal T cell homeostasis

Mark S. Ladinsky*, Leandro P. Araujo*, Xiao Zhang, John Veltri, Marta Galan-Diez†, Salima Soualhi†, Carolyn Lee, Koichiro Irie, Elisha Y. Pinker, Seiko Narushima, Sheila Bandyopadhyay, Manabu Nagayama, Wael Elhenawy, Brian K. Coombes, Ronaldo P. Ferraris, Kenya Honda, Iliyan D. Iliev, Nan Gao, Pamela J. Bjorkman‡, Ivaylo I. Ivanov‡

INTRODUCTION: Although commensal microbes populate our barrier surfaces without causing obvious disease, they nonetheless modulate host physiology and immunity. Commensal bacteria can regulate host T cell differentiation and function, and a large fraction of mucosal tissue-resident T cells are thought to recognize commensal antigens, which triggers the T cells' participation in the maintenance of mucosal homeostasis. Therefore, the mechanisms by which commensal antigens or other microbiota-derived immune mediators are acquired and processed to activate specific types of host T cells are of substantial interest. Understanding commensal-host communication and commensal antigen acquisition is crucial for understanding the mechanisms of tissue homeostasis and for the design of alternative strategies for specific regulation of mucosal health and pathologies.

RATIONALE: Host-microbe interactions at the cellular level have been almost exclusively studied in the context of invasive pathogens. Our study explored whether noninvasive com-

mensal microbes may possess previously unappreciated modes of antigen acquisition or communication with the host for maintenance of mucosal T cell homeostasis.

RESULTS: We examined the interaction of segmented filamentous bacteria (SFB), well-characterized T helper 17 ($T_{H}17$) cell-inducing epithelium-associated commensal microbes, with intestinal epithelial cells (IECs) by means of electron tomography. SFB were not phagocytosed by IECs and did not penetrate the IEC cytosol. SFB and IEC communicated through the generation of endocytic vesicles at the tip of the SFB-IEC synapse. The vesicles were released into the host IEC and contained an SFB cell wall-associated protein, which is a known immunodominant T cell antigen for the generation of mucosal $T_{H}17$ cells. Endocytic vesicles were present in virtually every SFB-IEC synapse in healthy animals, suggesting a highly dynamic process that occurs at steady state. SFB antigenic proteins were transferred through this process inside IECs and shuttled throughout the IEC endosomal-lysosomal

network. Mechanistically, the endocytic process was clathrin-independent but dependent on dynamin and the actin regulator cell division control protein 42 homolog (CDC42). Chemical inhibition of CDC42 activity in vivo led to disruption of the endocytosis. Genetic deletion of CDC42 in IECs resulted in disruption of endocytosis induced by SFB, loss of transfer of antigenic proteins inside IECs, and substantial decrease in the activation of SFB-specific CD4 T cells and SFB-induced $T_{H}17$ cell differentiation. An examination of a few other epithelium-associated or $T_{H}17$ cell-inducing intestinal microbes showed dissimilar interactions with IECs, and therefore, SFB currently are the first and only example of this process.

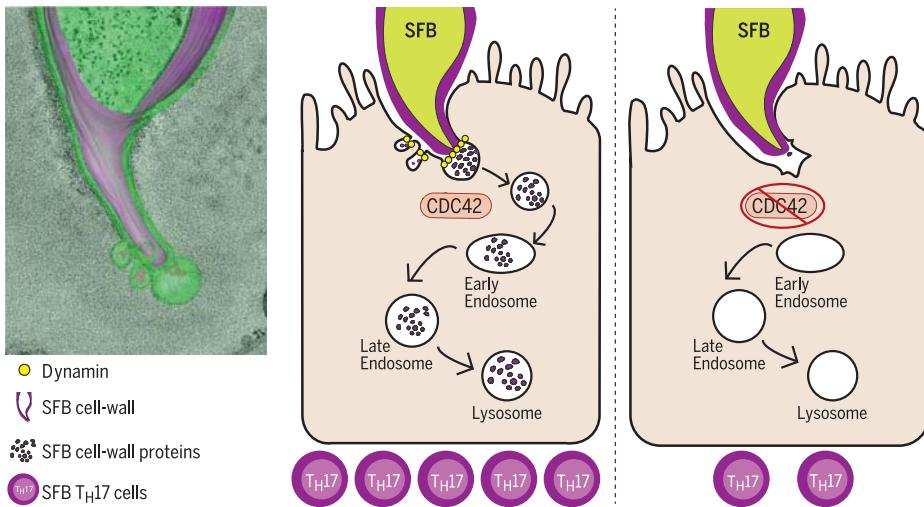
ON OUR WEBSITE

Read the full article at <http://dx.doi.org/10.1126/science.aat4042>

CONCLUSION: Our results reveal a mechanism of interaction between a commensal microbe and the host that directs transfer of microbial proteins inside host cells. They also describe a previously unappreciated pathway for antigen acquisition from luminal commensal bacteria through IECs. Our results underscore that the study of the interactions of key individual commensal microbes with the host may uncover unappreciated biological pathways. Targeting such pathways may allow for ways to specifically regulate commensal versus pathogenic interactions, regulate the immunomodulatory effects of individual members of the gut microbiota, or design alternative strategies for mucosal vaccination. ■

Downloaded from <http://science.sciencemag.org/> on May 13, 2020

SFB use microbial adhesion-triggered endocytosis (MATE) to transfer T cell antigens into IECs and modulate host T cell homeostasis. SFB interaction with IEC triggers formation of endocytic vesicles that contain proteins from the SFB cell wall. The vesicles enter host IEC through clathrin-independent and dynamin-dependent endocytosis. SFB proteins are shuttled through the IEC endosomal-lysosomal network and induce activation of lamina propria antigen-specific $T_{H}17$ cells. MATE, transfer of SFB antigenic proteins, and $T_{H}17$ activation depend on the actin cytoskeleton regulator protein CDC42.



RESEARCH ARTICLE

MICROBIOTA

Endocytosis of commensal antigens by intestinal epithelial cells regulates mucosal T cell homeostasis

Mark S. Ladinsky^{1*}, Leandro P. Araujo^{2*}, Xiao Zhang³, John Veltri⁴, Marta Galan-Diez^{2†‡}, Salima Soualhi^{2†§}, Carolyn Lee², Koichiro Irie^{2,5}, Elisha Y. Pinker², Seiko Narushima⁶, Sheila Bandyopadhyay³, Manabu Nagayama^{6,7}, Wael Elhenawy⁸, Brian K. Coombes⁸, Ronaldo P. Ferraris⁴, Kenya Honda^{6,9}, Illyan D. Iliev¹⁰, Nan Gao³, Pamela J. Bjorkman^{1¶}, Ivaylo I. Ivanov^{2||}

Commensal bacteria influence host physiology, without invading host tissues. We show that proteins from segmented filamentous bacteria (SFB) are transferred into intestinal epithelial cells (IECs) through adhesion-directed endocytosis that is distinct from the clathrin-dependent endocytosis of invasive pathogens. This process transfers microbial cell wall-associated proteins, including an antigen that stimulates mucosal T helper 17 ($T_{H}17$) cell differentiation, into the cytosol of IECs in a cell division control protein 42 homolog (CDC42)-dependent manner. Removal of CDC42 activity in vivo led to disruption of endocytosis induced by SFB and decreased epithelial antigen acquisition, with consequent loss of mucosal $T_{H}17$ cells. Our findings demonstrate direct communication between a resident gut microbe and the host and show that under physiological conditions, IECs acquire antigens from commensal bacteria for generation of T cell responses to the resident microbiota.

Commensal microbes are important modulators of host physiology, metabolism, and immunity. However, how they communicate with the host to achieve these effects is not well understood. Communication mechanisms between commensal and host cells may contain previously unappreciated

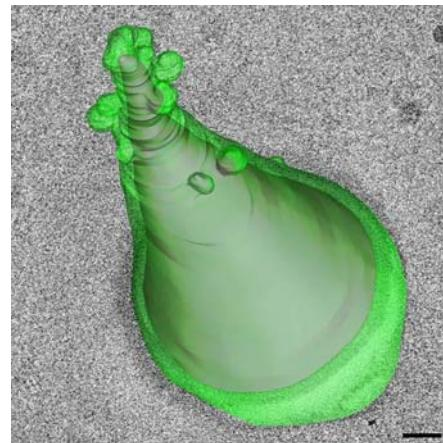
modes of host-microbe interaction. In contrast to pathogens, commensals do not normally invade host cells. Moreover, in the intestine, several host mechanisms—including secretion of mucus, immunoglobulin A (IgA), and antimicrobial peptides—prevent direct interaction with the host (7). Therefore, at steady state, most commensal microbes use indirect modes of communication with the host. These include, among others, release of immunostimulatory microbial products (such as lipopolysaccharide), secretion of microbial metabolites (such as short-chain fatty acids) or modification of host metabolites, and release of outer-membrane vesicles (2–6). Whether commensal bacteria have mechanisms to actively introduce microbial molecules into host cells to modify host physiology, and whether these mechanisms resemble known pathogen-host interaction pathways, is unknown. To identify communication pathways between commensal microbes and host cells, we performed structural and functional characterization of the interaction between segmented filamentous bacteria (SFB) and intestinal epithelial cells (IECs).

SFB are members of the resident gut microbiota in several animal species (7, 8). They are Gram-positive spore-forming bacteria of the class Clostridia (9, 10). SFB are immunomodulatory commensals and induce antigen-specific T helper 17 ($T_{H}17$) cells in a major histocompatibility complex class II (MHCII)-dependent manner (11–14). Despite this immune activation, SFB do not induce overt intestinal inflammation,

even in monocolonized mice, and are members of the commensal microbiota in most animal facilities (8, 15). In contrast to most commensal bacteria in laboratory mice (16), SFB associate with IECs (17, 18), and this association is crucial for the induction of SFB-specific $T_{H}17$ cells (19). The SFB genome lacks genes that encode any of the known bacterial injection-type secretion systems (9). Therefore, how the bacteria transport T cell antigens across the epithelial barrier or modulate IEC function is not known.

SFB and IECs communicate through endocytosis localized in the host-microbial synapse

We used electron tomography (ET) to reconstruct the SFB-IEC synapse in three dimensions. We first examined whether SFB is phagocytosed by IECs as previously suggested (20, 21). In agreement with earlier reports (20, 21), individual EM sections often showed presence of double-membrane phagosome-like vesicles containing microbial cytoplasm inside IECs (Fig. 1A, left). However, three-dimensional (3D) reconstruction by means of ET revealed that in all cases, these structures represent microbial cells located in deep invaginations of the IEC plasma membrane and that the bacteria remain entirely outside host cells (Fig. 1, A and B). In total, we examined more than 200 SFB-IEC synapses, and invasion of IEC cytosol or internalization of the bacterium was not present in any of them. We therefore conclude that SFB do not normally invade IECs. Instead, SFB form a hook-like holdfast (Fig. 1B) that we further characterized



Movie 1. Structure of the SFB-IEC synapse.

Electron tomogram and 3D reconstruction of an SFB-IEC synapse. Transverse serial planes of an SFB holdfast. The tomogram starts at the base of the holdfast and moves deeper into the IEC toward the tip of the holdfast, followed by 3D reconstruction of the whole volume. The bacterial and host membranes are uninterrupted throughout the length of the holdfast. 3D reconstruction colors are gray, SFB plasma membrane; magenta, SFB cytosol; and green, IEC plasma membrane. Scale bar, 100 nm.

by means of ET. 3D reconstruction of the synapse revealed existence of membrane vesicles at the distal end of the holdfast (Fig. 1C, Movie 1, fig. S1, and movie S1). The vesicles extended into the host cell cytoplasm and were present in almost all examined holdfasts, suggesting a dynamic process. The vesicles appeared to originate as uncoated blebs or pits mostly at the tips of holdfast segments (Fig. 1, C and D, and movie S1). In individual holdfasts, blebs formed vesicles with different levels of restriction of their membrane, including formation of necks (Fig. 1D), suggesting an active budding process. Indeed, free vesicles with similar density and morphology were detected inside the host IEC cytoplasm, close to holdfasts with actively budding blebs and near the vesicular network of the host cell (Fig. 1D and fig. S2). The vesicles originated exclusively from the host IEC plasma membrane and did not appear to include bacterial plasma membrane or cytoplasm (Fig. 1,

E to H; Movie 1; fig. S3; and movie S2). Individual bacteria-host synapses displayed an average of four vesicles that were mostly spherical, or slightly elongated, in shape and ~100 nm in diameter (Fig. 2, A to C). The origin, size, and morphology of the vesicles are consistent with the classical definition of endocytosis. Because the endocytic vesicles were exclusively present at the microbial-host synapse, we termed the process microbial adhesion-triggered endocytosis (MATE) and further examined its role in immune modulation by the bacteria.

MATE is a specific communication between SFB and the host that transports SFB-derived T cell antigens inside IECs

MATE vesicles were present with normal morphology in SFB-colonized NOD-*Scid*.*Il2rg*^{−/−} (NSG) mice, which are immunodeficient and lack B cells, T cells, natural killer cells, and in-

nate lymphoid cells (Fig. 2, A to C), demonstrating that MATE is not dependent on the immunomodulatory functions of SFB.

We next examined whether MATE may represent a previously unappreciated mode of communication between the microbe and host cells. Tomographic reconstruction of MATE vesicles showed that they often contained electron-dense cargo (Figs. 1, C and F, and 2, D and E, and movies S1 and S2). We asked whether this cargo was of bacterial origin. SFB induce an antigen-specific CD4 T_H17 cell response (13, 14), and a substantial component of this response is directed against the SFB protein P3340 (14). P3340 lacks a transmembrane domain and is predicted to be extracellular (14). We found that P3340 localizes exclusively to the SFB cell wall on the surface of the microbe (Fig. 2F). In SFB-IEC holdfasts, P3340 was also present in MATE vesicles (Fig. 2, G and H). Moreover, P3340 was present in vesicles inside the cytoplasm

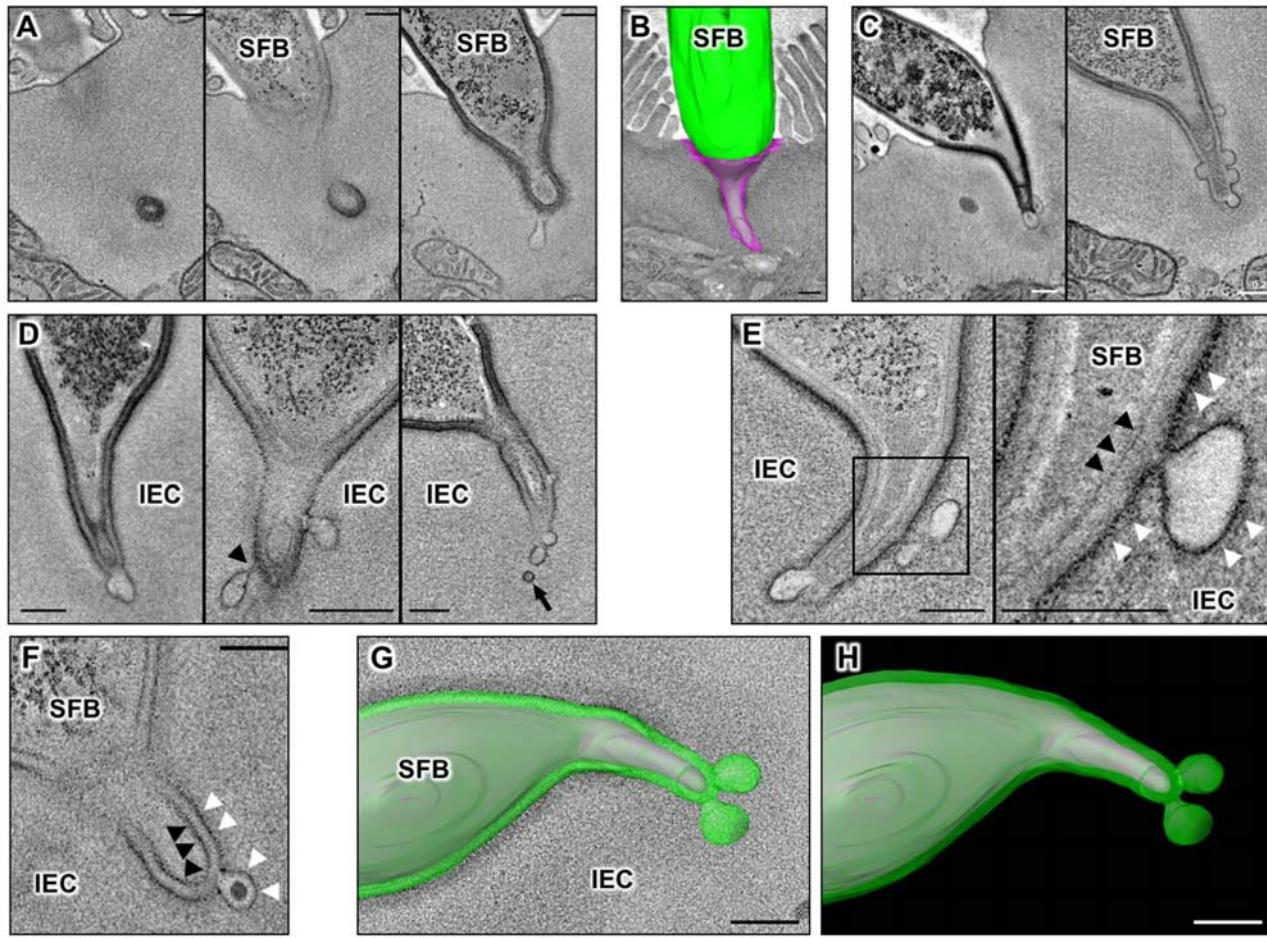


Fig. 1. MATE is induced after attachment of commensal SFB to IECs. (A) Consecutive sections of an electron tomogram of an SFB-IEC synapse showing that double-membrane phagosome-like vesicles (left) represent invaginations of the IEC plasma membrane. (B) A 3D reconstruction of an SFB-IEC holdfast, demonstrating separation of the IEC plasma membrane (PM) in purple and the SFB PM in green. SFB do not penetrate the IEC PM.

(C) Membrane vesicles at the tip of SFB holdfasts. (D) Holdfast vesicles form necks (arrowhead) and bud off (arrow) from the IEC PM into the IEC cytosol. (E and F) SFB PM (black arrowheads) remains uninterrupted, and holdfast vesicles form exclusively from the host IEC PM (white arrowheads) and contain electron dense cargo (F). (G and H) Reconstruction of an SFB holdfast. IEC PM is in green, and SFB PM is in gray. Scale bars, 200 nm.

of IECs that contained attached SFB (Figs. 2, G to I, and 3, A and B). To examine the nature of these vesicles, we costained tissue sections from the terminal ileum with various endocytic markers. Intracellular P3340 could be detected

in multiple vesicular compartments, including apical EEA1-positive early endosomes (Fig. 3, C and D), Rab7- or lysobisphosphatidic acid (LBPA)-positive late endosomes, and basolateral LAMP2-positive lysosomes (Fig. 3, E to H).

These data show that P3340 is shuttled throughout the endosome/lysosome vesicular pathway of IECs. Therefore, MATE represents a pathway that transports an immunodominant commensal protein inside IECs at steady state.

To investigate whether MATE mediates communication of other intestinal bacteria with the host, we examined microbiota-host interactions in specific-pathogen-free (SPF) mice from the Jackson laboratory that lack SFB (11). Despite the presence of a large and diverse microbial community, none of the commensal microbes in Jackson mice interacted directly with IECs (Fig. 4A). We next used ET to examine the interactions of several defined microbes with the intestinal epithelium. *Citrobacter rodentium* and adherent-invasive *Escherichia coli* (AIEC) are intestinal pathogens that interact directly with the gut epithelium. For *C. rodentium*, intimate contact with IECs is mediated by a type III secretion system (T3SS). Indeed, needlelike structures linking bacterial and host cells were apparent by ET in tissues infected with *C. rodentium* (Fig. 4, D to F). AIEC were found in the gut lumen contacting IEC microvilli or internalized inside IECs (Fig. 4, B and C). However, neither *C. rodentium* nor AIEC used MATE to interact with IECs (Fig. 4, B to F). We also examined human T_H17 cell-inducing microbes that are known to reside close to IECs. Neither *Bifidobacterium adolescentis* (22) nor a mixture of 20 human T_H17-inducing bacteria (19) used MATE for communication with the host (Fig. 4, G and H). Although some of these organisms contacted IEC microvilli, most did not directly engage IECs. Therefore, MATE appears to be a specific mode of communication between SFB and the host and is not a general property of the commensal, epithelium-adherent, or T_H17-inducing bacteria we examined.

MATE is clathrin-independent and CDC42-dependent

We next investigated the molecular mechanism of MATE. Clathrin coating was not present on MATE vesicles (Fig. 5, A to D). Moreover, treatment of externalized intestinal loops with the clathrin-dependent endocytosis inhibitor Pitstop 2 blocked clathrin-dependent endocytosis of fluorescently labeled IgG (fig. S4) but did not affect the morphology of MATE vesicles (Fig. 6, C to F, and fig. S6). By contrast, treatment with Dynasore, an inhibitor of dynamin, disrupted vesicle morphology, resulting in enlarged vesicles (Fig. 6, C to F). Dynamin is a large guanosine triphosphatase (GTPase) that forms helices around the necks of nascent endocytic vesicles and participates in vesicle scission. High-resolution ET revealed presence of helical protein rings around nascent necks of MATE vesicles, strongly resembling dynamin rings (Fig. 5, E to G). On the basis of these data, we conclude that MATE is clathrin-independent and dynamin-dependent. We next searched for specific molecular mediators of MATE. Actin polymerization has been reported around the SFB-IEC synapse (23). We found an obvious actin cytoskeleton reorganization of the IEC

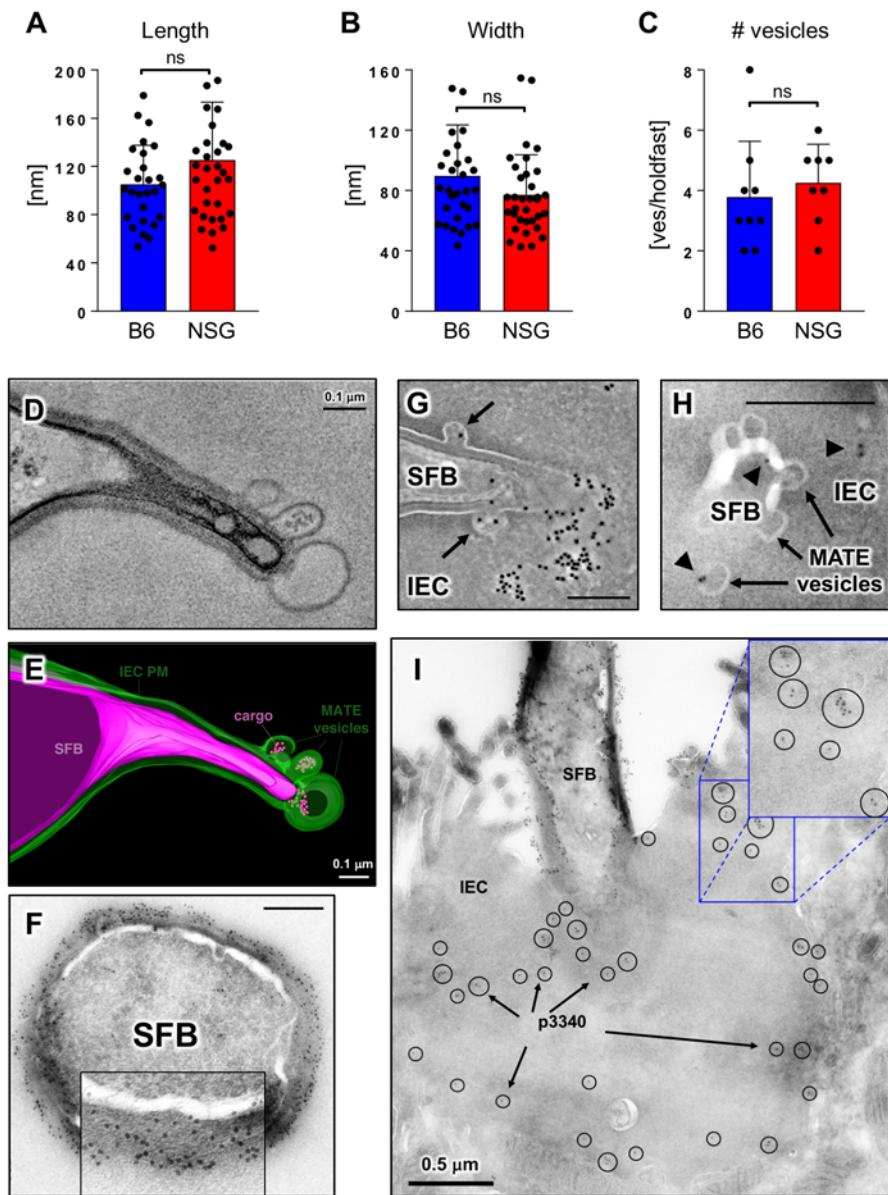


Fig. 2. MATE vesicles transfer an immunodominant SFB antigen inside IECs. (A to C) Quantification of [(A) and (B)] MATE vesicle size and (C) numbers per holdfast in the terminal ileum of C57BL/6J (B6) and NOD.Scid.II2rg^{null} (NSG) mice. Error bars, standard deviation. Statistics, unpaired two-tailed *t* test. (D and E) Single section and 3D reconstruction of an SFB-IEC synapse featuring MATE vesicles that contain electron-dense cargo. Green, IEC PM; magenta, SFB PM. (F) Immuno-EM for P3340 on SFB in mouse intestine. Cross section of an SFB cell. P3340 is present exclusively on the cell-wall of the bacterium. (G, H, and I) Immuno-EM for P3340 on intestinal sections from terminal ileum. (G) An SFB cell interacting with a single IEC transfers P3340 into the IEC cytosol via MATE. Arrows, MATE vesicles containing P3340 labeling. (H) A close-up of the distal end of an SFB holdfast showing P3340 presence (black arrowheads) on the microbe, in a MATE vesicle, and inside the IEC cytosol. (I) Immuno-EM of P3340 in terminal ileum of C57BL/6J mice colonized with SFB. An IEC with an attached SFB is shown. P3340 immunogold labeling is present on the cell wall of the bacteria, as well as inside the IEC cytosol in the vicinity of the SFB-IEC synapse (black circles and arrows). Scale bars, 200 nm (unless otherwise noted).

cytoplasm in the immediate vicinity of holdfast segments. This included reorganization of the terminal web and formation of an organelle-free zone (OFZ) immediately around holdfasts (Fig. 5, H and I). Therefore, we examined whether regulators of actin may be involved in MATE. CDC42 (cell division control protein 42 homolog) is a small GTPase of the Rho family that plays a central role in regulating both actin cytoskeleton dynamics and vesicular trafficking, including certain endocytic pathways (24). We found that SFB colonization induces CDC42 activation in IECs in the terminal ileum (Fig. 6, A and B, and fig. S5). Moreover, treatment of externalized intestinal loops from SFB-colonized NSG mice with CASIN (CDC42-specific inhibitor) strongly affected MATE vesicle morphology (Fig. 6, C to F). CASIN-treated loops contained a similar number of SFB synapses and a similar number of MATE vesicles per synapse (fig. S6). However, after CASIN treatment, MATE vesicles increased in size and appeared arrested at the synapse (Fig. 6, C to F). We therefore conclude that CDC42 activity is required for the proper progression of MATE.

Epithelial CDC42 is required for MATE, transfer of SFB antigens, and SFB-specific T_H17 cell activation

Inhibition of CDC42 activation in intestinal loops interfered with MATE; hence, we examined whether epithelial CDC42 is required for the immunomodulatory effects of SFB and, particularly, activation of SFB-specific CD4 T cells. We generated mice with an IEC-specific deletion of CDC42 by crossing CDC42-flox mice with Villin-Cre animals (IEC^{ΔCDC42} mice). IEC^{ΔCDC42} mice show defects in epithelial cell morphogenesis and remain smaller than their littermates (25). However, the mice are viable, survive into adult-

hood, and do not develop intestinal inflammation (25). SFB successfully colonized IEC^{ΔCDC42} mice, and SFB attachment to IECs and holdfast formation in the absence of epithelial CDC42 was similar to those in littermate controls (Fig. 7A). However, there was a significant expansion of SFB in the intestinal lumen of IEC^{ΔCDC42} mice (Fig. 7B), suggesting disrupted host immune response. MATE vesicle formation was impaired in the absence of CDC42, and MATE vesicles were much smaller in IEC^{ΔCDC42} mice (Fig. 7C and fig. S7). Transfer of the MATE-derived SFB antigen P3340 into IECs was greatly reduced in the absence of epithelial CDC42 (Fig. 7D). Moreover, despite an increase in luminal SFB levels, IEC^{ΔCDC42} mice had decreased levels of interleukin-17 (IL-17) mRNA in terminal ileum (Fig. 7E) and a substantial decrease in T_H17 cells in the small intestinal lamina propria (Fig. 7, F and G). At the same time, induction of IgA production by SFB was not significantly affected (fig. S8), which argues that CDC42 deficiency did not affect all aspects of SFB immune modulation. Transcriptional profiling of IECs from control and IEC^{ΔCDC42} mice revealed that many SFB-induced epithelial genes were not significantly, or only slightly, affected by the absence of CDC42, demonstrating that epithelial cell function was not universally perturbed (Fig. 7H and figs. S9 and S10). Moreover, many epithelial genes associated with T_H17 cell induction by SFB—such as *Reg3g*, *Saa1*, *Saa2*, *Saa3*, *Nos2*—were not significantly affected in IEC^{ΔCDC42} mice (Fig. 7, H to K, and figs. S9 and S10). We therefore hypothesized that the loss of T_H17 cells in the absence of epithelial CDC42 and MATE is due mainly to a decrease in SFB antigen acquisition through IECs.

To test whether MATE transports SFB antigens through IECs for T cell activation in a

CDC42-dependent fashion, we examined the effects of epithelial CDC42 deletion on the activation of SFB-specific CD4 T cells. To address developmental defects in IEC^{ΔCDC42} mice, we crossed CDC42-flox animals to Villin-Cre-ER mice to allow for conditional deletion of CDC42 in adulthood. The resulting IEC^{ΔCDC42-CKO} mice develop normally in the absence of tamoxifen treatment. We deleted epithelial CDC42 in adult IEC^{ΔCDC42-CKO} mice before colonization with SFB and transfer of 7B8 Tg CD4 T cells, specific for the SFB antigen P3340 (14). Tamoxifen treatment led to interference with the generation of MATE vesicles in IEC^{ΔCDC42-CKO} mice, similarly to IEC^{ΔCDC42} mice (Fig. 8A and fig. S7). IEC^{ΔCDC42-CKO} mice showed significant decrease in the induction of endogenous intestinal T_H17 cells (Fig. 8, B to F), especially the induction of V β 14⁺ T_H17 cells (Fig. 8, B and D), which are enriched in SFB specificities and P3340-specific TCRs (13, 14, 26). In addition, expansion and proliferation of adoptively transferred P3340-specific 7B8 Tg T cells was significantly reduced in IEC^{ΔCDC42-CKO} mice compared with control tamoxifen-treated recipients (Fig. 8, G to I), demonstrating decreased availability of SFB antigens, and particularly P3340, in the absence of MATE. Induction of SFB-specific T_H17 cell responses occurs normally in Peyer's Patch-deficient mice (13, 27). Accordingly, proliferation of 7B8 Tg T cells was unaffected, and even slightly increased, in Peyer's Patch-deficient mice in which ROR γ (RAR-related orphan receptor- γ) was knocked out (fig. S11), which argues that CDC42 activity is not crucial for SFB antigen sampling by M cells. Combined, these data demonstrate that MATE delivers commensal-derived antigens via IECs in a CDC42-dependent manner for the optimal induction of antigen-specific CD4 T cell responses.

Conclusion

We have identified MATE as a distinct mode of microbe-host interaction that involves transfer of cell wall-associated bacterial proteins into host cells by using clathrin-independent, dynamin-dependent, CDC42-dependent endocytosis after establishment of a cell-cell contact. MATE vesicles likely correspond to the “rounded protrusions” reported by Chase and Erlandsen more than 40 years ago (28). In contrast to internalization of microbial pathogens, bacterial plasma membranes appeared uninterrupted in all of the SFB-IEC holdfasts that we examined, and we did not detect any evidence for direct transfer of bacterial cytosol into the host cell. How bacterial proteins enter MATE vesicles remains unclear. This could be an active process, involving secretory machinery or a passive acquisition of microbial cell wall proteins. In agreement with the latter, we observed direct contact between nascent MATE vesicles and the SFB cell wall (fig. S12). Thus, in addition to P3340, we expect other cell wall-associated SFB proteins to be present in MATE vesicles and activate mucosal CD4 T cells. IECs can endocytose entire commensal microbes under conditions of intestinal

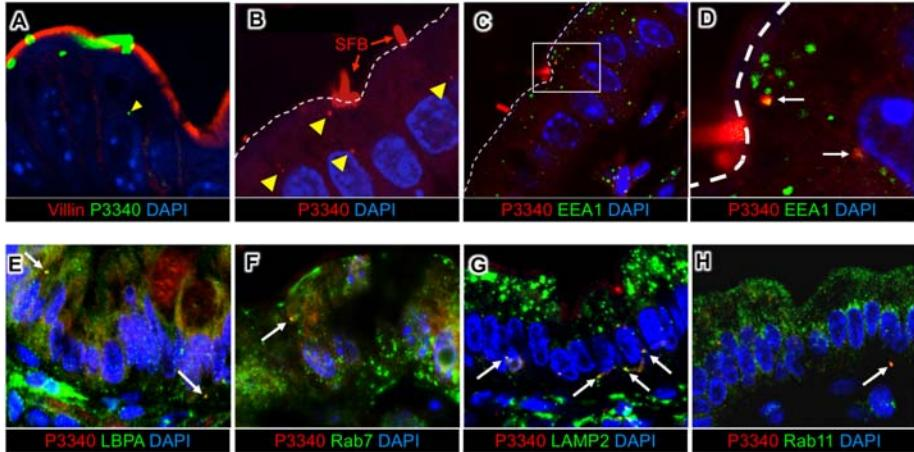


Fig. 3. SFB antigens are shuttled through the IEC endosomal-lysosomal vesicular network. (A and B) Immunofluorescence for P3340 on intestinal sections from terminal ileum showing SFB P3340 inside IECs (yellow arrowheads). (C and D) P3340 is present in EEA1⁺ early endosomes. White dashed line outlines the apical IEC surface. (E to H) Colocalization of intracellular SFB protein P3340 (red) with endosomal and lysosomal markers (green). P3340 colocalizes with [(E) and (F)] late endosomes (LBPA and Rab7), as well as (G) basolateral lysosomes (LAMP2). (H) Some P3340 also colocalizes with recycling endosomes (Rab11).

inflammation or dysbiosis (29). However, whether and how commensal microbes interact with host cells at steady state has not been examined. We found that MATE transfers antigens from SFB into IECs, and this contributes to generation of

both commensal-specific CD4 T cell responses and generation of commensal-specific homeostatic T_H17 cells. This process occurs under physiological conditions in normal SPF animals. Several details of the SFB antigen presentation

pathway remain to be elucidated. We previously showed that SFB-specific T cell responses require intestinal macrophages (26). Here, we show that SFB antigens are introduced into IECs. Inside IECs, SFB antigens are present throughout the endosomal/lysosomal compartment, including at the basolateral side of IECs. It is therefore possible that SFB antigens are processed in IECs or simply transported through IECs to the lamina propria, where they are acquired by intestinal macrophages. Alternatively, IECs may directly introduce SFB antigens into intestinal macrophages—for example, through phagocytosis of apoptotic IECs (30). Our study identifies IECs as important innate immune cells in the acquisition of SFB antigens and initiation of SFB-specific T cell responses.

Together with previous studies, our results show that host-microbe interactions in the gut occur on a spectrum. This spectrum ranges from “immunological ignorance” of luminal commensals (1, 31) to inflammation and tissue damage caused by invasive pathogens. It also includes immunomodulatory resident microbes, such as regulatory T cell-inducing mucus-associated bacteria (32, 33) and epithelium-associated T_H17-inducing microbes (11, 19). The specific mechanisms that control interactions with microbes at different levels of this spectrum are crucial for maintenance of mucosal homeostasis. MATE represents a previously unidentified communication pathway that contributes to the sampling of commensal antigens. This sampling occurs at steady state, in the absence of an inflammatory response, and is mechanistically distinct from the internalization of conventional pathogens. Although we were unable to identify additional examples of MATE, other epithelium-associated members of the normal microbiota are currently not known. We therefore predict that discovery of additional epithelium-associated microbiota species will bring further examples of MATE or similar processes. Our results underscore the importance of studying individual commensal microbes for identification of alternative modes of host-microbe communication. Moreover, targeting such pathways, including MATE, may allow for ways to specifically regulate commensal versus pathogenic interactions or regulate the immunomodulatory effects of individual members of the gut microbiota. It may also represent an alternative strategy for antigen delivery for mucosal vaccination or modulation of IEC function.

Materials and methods

Animals

C57BL/6J, Balb/cJ and NOD.*Scid.II2rg*^{null} (NSG) mice were obtained from the Jackson Laboratory. Villin-Cre (Stock No 004586) on C57BL/6 background were obtained from the Jackson laboratory. 7B8-TCR-Tg mice (14) were a kind gift from Dr. Dan Littman, NYU. CDC42-floxed mice on C57BL/6 background (34) were a kind gift from Dr. Yi Zheng, Cincinnati Children's Hospital Medical Center. Vil-Cre-ER mice (35) were a kind gift from Dr. Sylvie Robine, Institut Curie. All non-commercial mouse strains were

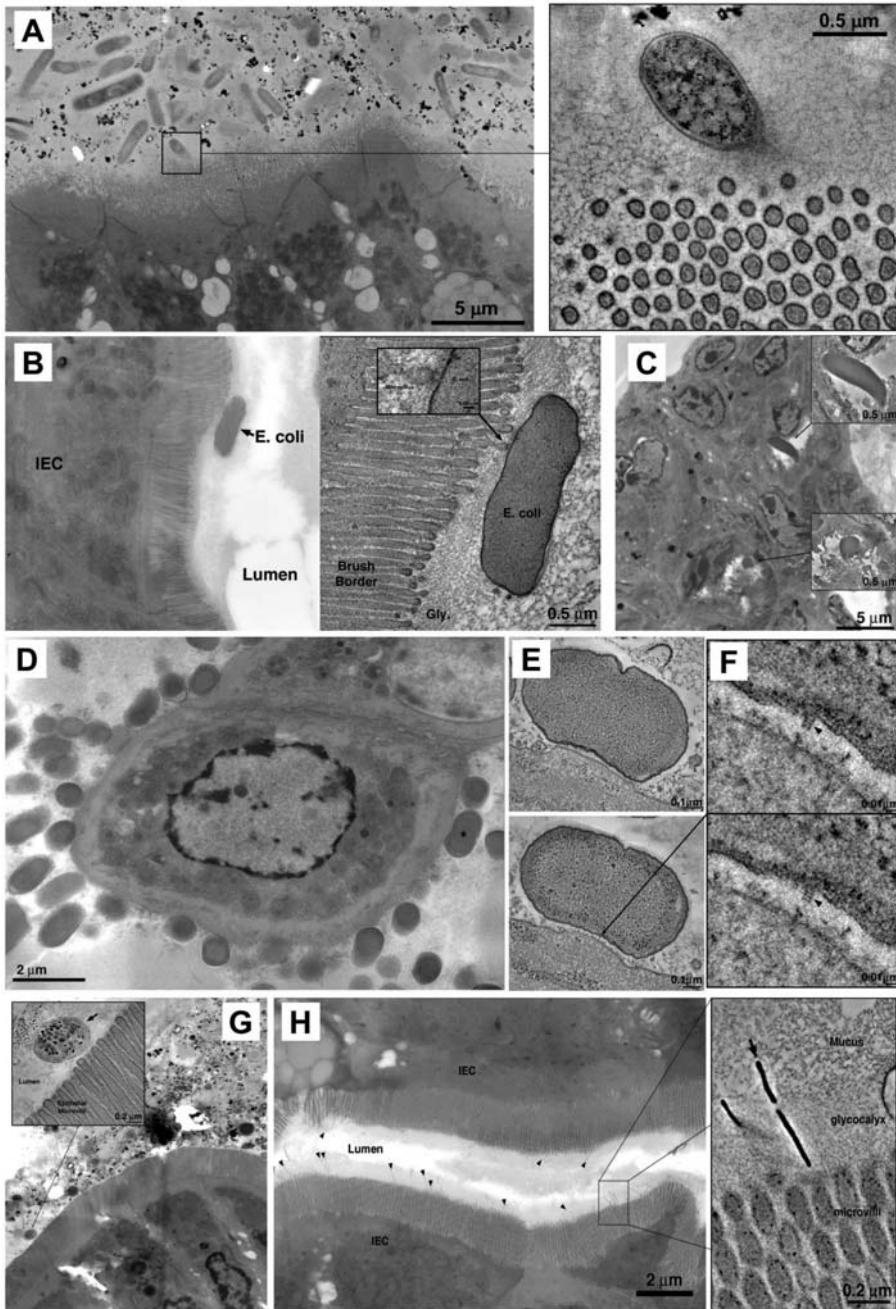


Fig. 4. Electron tomography of host-microbe interactions in the intestine. (A) Microbiota in the terminal ileum of SFB-negative Jackson C57BL/6J mice possess limited interactions with IECs and lack MATE. (Inset) Rare interaction between a bacterial cell and IEC microvilli. (B and C) Interactions of AIEC strains (B) LF82 and (C) NRG857c with IECs in terminal ileum. [(B), right] Tomogram showing interaction with microvilli. (C) Internalized AIEC cells. (D) *C. rodentium*, overview showing numerous bacterial cells associating with IEC surface in the colon. (E) Tomograms of a *Citrobacter* pedestal. (F) Tomographic details of a presumptive T3SS needle connecting the microbe to IEC (arrowheads). (G) Mixture of 20 human T_H17 cell-inducing strains. (Inset) Tomogram showing bacterial cells in the lumen, close to microvilli, but not making contact with IECs. (H) *B. adolescentis* (arrowheads) in terminal ileum. (Inset) Tomogram of *B. adolescentis* showing penetration of the glycocalyx and interaction with the IEC microvilli.

re-derived SPF at the Jackson Laboratory. All mouse strains were bred and housed under SPF conditions at Columbia University Medical Center under IACUC approved guidelines. To control for microbiota and cage effects, experiments were performed with gender matched littermate control animals that were housed in the same cage whenever possible. Littermate

controls of IEC^{ΔCDC42} mice included a mixture of (F/+), VilCre), (F/F, Non), and (F/+), Non genotypes.

SFB colonization and fecal SFB quantification

SFB colonization was performed by oral gavage with SFB-containing fecal pellets. The source of

SFB was from Taconic C57BL/6 mice from location IBU17. SFB colonization levels were confirmed by quantitative polymerase chain reaction (PCR) of fecal bacterial DNA and normalized to levels of total bacteria (UNI) as previously described (16).

Gnotobiotic mice with T_H17 cell inducing microbiota

A consortium of 20 human T_H17-inducing bacteria was originally isolated from a stool sample of a Japanese ulcerative colitis patient as described previously (19). Bacterial strains were individually grown in either PYG broth or reinforced Clostridial broth (Oxoid, CM0149) under strictly anaerobic conditions (80% N₂, 10% H₂, 10% CO₂) at 37°C in an anaerobic chamber (Coy Laboratory Products) overnight, adjusted to the same OD values, mixed, and the cocktail inoculated into four germ-free (GF) mice by oral gavage. *B. adolescentis* was isolated from ileal mucosal biopsy specimens collected by double-balloon enteroscopy from a patient with Crohn's disease. The study was approved by the Ethics Committee of Jichi Medical University Hospital (#A14-196), and a written informed consent was obtained from the patients. Biopsy specimens were disrupted by pipetting and plated onto several media (EG, LBS, RCM, BL, GAM, MRS) under strictly anaerobic conditions at 37°C in an anaerobic chamber. Three out of seven colonies grown on LBS agar were identified as *B. adolescentis* based on the 16S rRNA gene sequences. For generating *B. adolescentis*-monocolonized mice, *B. adolescentis* was cultured overnight in CM0149 medium and administered into GF mice by oral gavage. Colonization of the bacteria was confirmed by Gram staining of fecal smear. Three to four weeks after the inoculation, terminal ileum segments (0.5 to 1.0 cm) were extracted from gnotobiotic mice, immediately placed into 2-ml tubes filled with ice-cold ET fixation solution (see below), and shipped refrigerated to Caltech for processing and imaging.

C. rodentium and AIEC colonization

For *Citrobacter* infection, 1 × 10⁹ CFU of *Citrobacter rodentium* were introduced into C57BL/6J mice by oral gavage. Colon samples were collected on Day 7 post infection. For AIEC infections, C57BL/6J mice were pre-treated with streptomycin 24 hours prior to infection with 1 × 10⁹ CFU of AIEC strain LF82 or AIEC strain NRG857c. For LF82 infection, mice were also treated with ampicillin in drinking water for the duration of the experiment. Terminal ileum samples were collected on Day 2 post infection, fixed in ice-cold ET fixation solution, and shipped to Caltech for processing and imaging.

Electron tomography and quantification of MATE vesicles

Terminal ileum segments (0.5 to 1 cm) were extracted from SFB-containing mice and immediately prefixed with ice-cold ET fixation solution 3% glutaraldehyde, 1% paraformaldehyde, 5% sucrose in 0.1 M sodium cacodylate trihydrate.

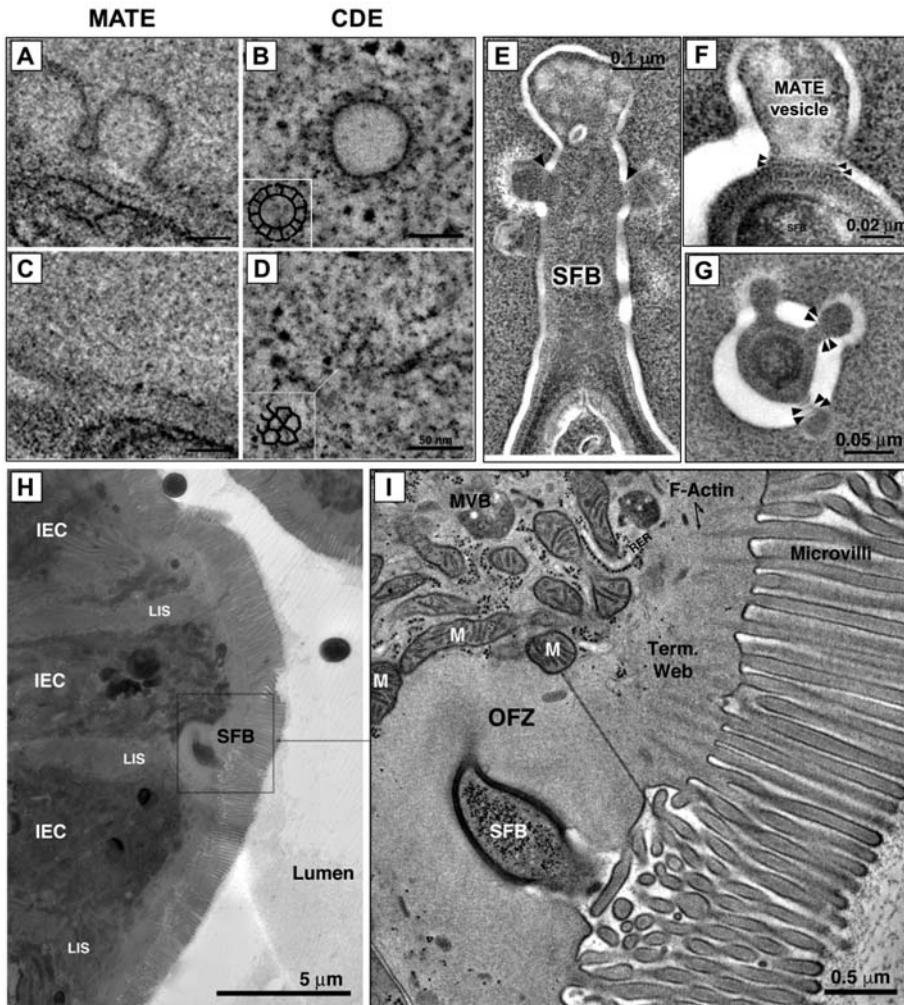


Fig. 5. MATE is a type of clathrin-independent endocytosis. (A to D) MATE vesicles do not contain clathrin coat. Tomographic reconstruction of [(A) and (C)] MATE vesicles and [(B) and (D)] clathrin-coated vesicles in cultured HeLa cells. [(A) and (B)] Tomographic slices taken near the equator of the vesicle. Clathrin spikes (arrows) are present on the surface in (B) but absent in (A). [(C) and (D)] Tomographic slices taken at the surface of the vesicles, showing clathrin cage composed of triskelions in (D) and lack of coating in (C). (Insets) Manual segmentation of the clathrin cage to highlight its features. (E to G) MATE vesicles contain dynamin-like rings. (E) Tomographic slice of an SFB holdfast interacting with an intestinal epithelial cell, showing thin bands (arrowheads) circumscribing the necks of MATE vesicles. [(F) and (G)] High-magnification details from negative-stain tomograms showing MATE vesicles in (F) longitudinal and (G) cross section. Dynamin-like bands are clearly visible circumscribing the necks of the vesicles (arrowheads). (H and I) SFB induce reorganization of the IEC actin cytoskeleton. An (H) overview and (I) magnification showing an interaction between SFB and an intestinal epithelial cell (IEC) in the terminal ileum. Reorganization of actin filaments in the IEC terminal web is evident immediately around the SFB holdfast. This reorganization seems to result in an OFZ. The demarcation between normal terminal web and the OFZ is noted by a thin double-dashed black line in (I). The OFZ contains vesicles and actin filaments organized differently than the terminal web in the neighboring area. LIS, lateral intercellular space; MVB, multivesicular body; M, mitochondrion.

Within 24 hours the tissue samples were rinsed with fresh 0.1 M cacodylate buffer and placed in brass planchettes (Type A; Ted Pella, Redding, CA) prefilled with 10% Ficoll in cacodylate buffer. The samples were covered with the flat side of a Type-B brass planchette and cryoimmobilized with a HPM-010 high-pressure freezing machine (ABRA Fluid AG, Windau, Switzerland). The vitrified samples were transferred immediately under liquid nitrogen to cryotubes (Nunc) containing a frozen solution of 2.5% osmium tetroxide, 0.05% uranyl acetate in acetone. Tubes were loaded into an AFS-2 freeze-substitution machine (Leica Microsystems) and processed at -90°C for 72 hours, warmed over 12 hours to -20°C, held at that temperature for 8 hours, then warmed to 4°C for 1 hour. The fixative was removed and the samples rinsed 4× with cold acetone, following which they were infiltrated with Epon-Araldite resin (Electron Microscopy Sciences, Port Washington PA) over 48 hours, flat-embedded between two Teflon-coated glass microscope slides and polymerized at 60°C for 24 to 48 hours.

Flat-embedded tissues were observed with a stereo dissecting microscope. Suitable regions were extracted with a scalpel, oriented to optimize access to villus tips, and glued onto plas-

tic sectioning stubs. Semi-thick (400 nm) serial sections were cut with a UC6 ultramicrotome (Leica Microsystems) using a diamond knife (Diatome, Switzerland). Sections were placed on Formvar-coated copper-rhodium slot grids (Electron Microscopy Sciences) and stained with 3% uranyl acetate and lead citrate. Gold beads (10 nm) were placed on both surfaces of the grid to serve as fiducial markers for subsequent image alignment. Grids were placed in a dual-axis tomography holder (Model 2040, E.A. Fischione Instruments, Export PA) and imaged with a Tecnai TF30ST-FEG transmission electron microscope (300 KeV) equipped with a 2k × 2k CCD camera (XP1000; Gatan, Pleasanton, CA). Tomographic tilt-series and large-area montaged overviews were acquired automatically using the SerialEM software package (36). For tomography, samples were tilted ±64° and images collected at 1° intervals. The grid was then rotated 90° and a similar series taken about the orthogonal axis. Tomographic data was calculated, analyzed and modeled using the IMOD software package (37, 38) on MacPro computers (Apple, Cupertino, CA). Quantification of MATE vesicles was performed by measuring individual vesicles' length and width. Length (L) was defined as the

longest distance from the connection of the vesicle with the IEC plasma membrane to the tip of the vesicle. Width (W) was measured in the same tomographic slice and defined as the largest distance between vesicle membranes perpendicular to L .

Immuno-electron microscopy

Terminal ileum segments (0.5 to 1 cm) were extracted from SFB-containing mice and immediately prefixed with ice-cold 4% paraformaldehyde, 5% sucrose in 0.1 M sodium cacodylate trihydrate. Within 24 hours, the tissues were rinsed with cacodylate buffer, cut into ~0.5 mm³ blocks and infiltrated with 2.1 M sucrose in cacodylate buffer over 24 hours. Individual blocks were affixed to aluminum cryo-sectioning stubs and rapidly frozen in liquid nitrogen. Thin (100 nm) cryo-sections were cut with an UC6/FC6 cryo-ultramicrotome (Leica Microsystems) using a cryo-diamond knife (Diatome) with a 35° included angle. Cryo-sections were transferred with a wire loop to Formvar-coated, carbon-coated, glow-discharged copper/rhodium 100-mesh EM grids and placed in PBS. Sections were incubated for 30 min in 10% calf serum in PBS to block nonspecific antibody binding, then incubated with primary antibodies diluted in PBS with 5% calf serum for 2 hours. After 4 rinses with PBS, the sections were incubated for 2 hours with colloidal gold conjugated secondary antibodies specific to the host animal of the primary, also diluted in PBS + 5% calf serum. Sections were then rinsed 4× with PBS, 4× with dH₂O, negatively stained with 1% uranyl acetate and stabilized with 1% methylcellulose. Immunolabeled samples were imaged and analyzed as described above.

Immunofluorescence and quantification of P3340 intracellular vesicles

For immunofluorescence, terminal ileum sections were fixed in 4% paraformaldehyde (PFA) and embedded in paraffin for anti-P3340 staining. Polyclonal rabbit anti-P3340 (14) was a gift from D. Littman, NYU. In some experiments, sections were costained with fluorescently labeled antibodies against EEA1 (#sc-137130, Santa Cruz), Rab7 (#R8779, Sigma), LBPA (#MABT837, Millipore), LAMP2 (#ABL-93-s, DSHB) or Rab11 (#610656, BD Biosciences). Image acquisition was performed on Nikon Ti Eclipse or Zeiss inverted confocal microscopes. Quantifications of intracellular P3340 vesicles were based on counts in 11 independent villi for each genotype.

Treatment with chemical inhibitors in externalized intestinal loops

NSG mice contain an expanded SFB population in the intestinal lumen as previously reported (39). In addition, NSG mice contained greatly increased number of SFB-IEC synapses. Therefore, SFB-IEC synapses were much easier to detect by ET in NSG than in B6 mice. Because of this feature, and because the morphology and frequency of MATE vesicle were unaffected in NSG mice (Fig. 2A), intestinal loop inhibitor

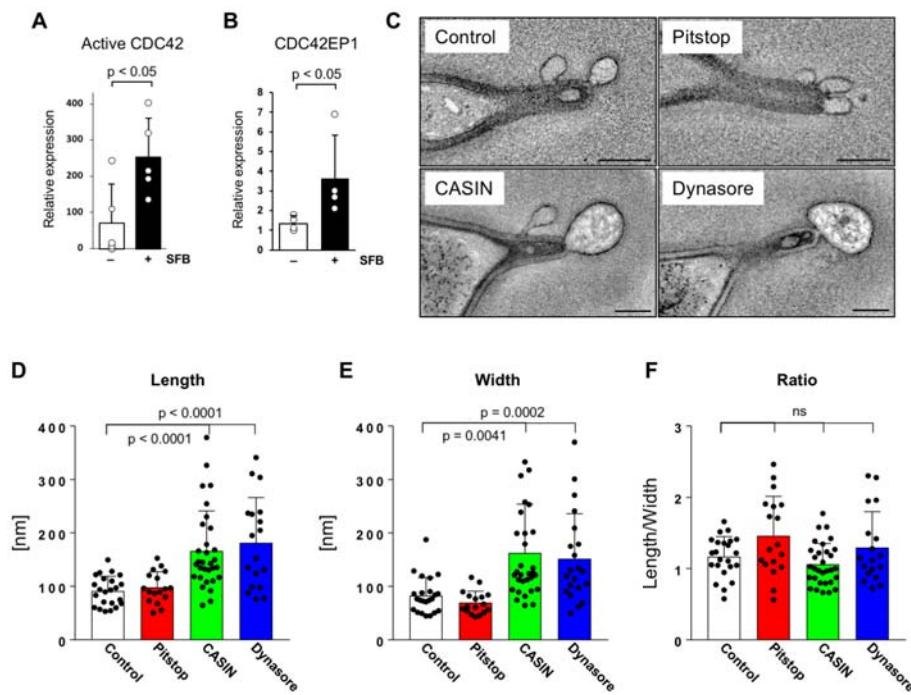


Fig. 6. MATE is CDC42-dependent and dynamin-dependent. (A and B) Quantification of active CDC42-GTP and CDC42EP1 expression in IECs isolated from terminal ileum of C57BL/6J mice 10 days after colonization with SFB. CDC42-GTP levels in (A) were normalized to total CDC42, and CDC42EP1 levels in (B) were normalized to β-actin. Data points represent individual animals. (C to F) MATE is CDC42-dependent and dynamin-dependent. NSG mice were colonized with SFB for at least 1 month. After establishment of persistent colonization, chemical inhibitors were introduced into externalized terminal ileum intestinal loops of live animals by means of perfusion *in vivo*, as described in Materials and methods. (C) Representative electron tomograms of SFB-IEC synapses. Scale bars, 200 nm. [(D) to (F)] Quantification of MATE vesicle morphology. Data points represent individual MATE vesicles. All error bars, standard deviation. Statistics, (A) and (D) to (F) unpaired two-tailed *t* test, (B) Mann-Whitney-Wilcoxon test.

experiments were performed in NSG mice. Perfusion of extraintestinal loops was done as previously described (40). Briefly, NSG mice were colonized with SFB from Taconic B6 mice for at least one month. Mice were anesthetized using ketamine (40 mg/kg) and xylazine (5 mg/kg). A

3 cm portion of the terminal ileum just proximal from the caecum was exteriorized and the contents flushed. The externalized portion was perfused with the inhibitors for 30 min using a syringe pump (Harvard Apparatus Model 22, Cambridge, MA, USA) via a Tygon tube through

jacketed water baths (37°C, VWR Scientific Model 1162) and into a steel catheter surgically attached to the proximal incision. Animals were perfused with 20 μM Pitstop 2 (SIGMA SML 1169), 10 μM CASIN (SIGMA SML 1253), 50 μM Dynasore (SIGMA D7693), or buffer. As positive control for the Pitstop 2 treatment, animals were perfused with 40 μg/ml Cy3-IgG (#015-160-003, Jackson ImmunoResearch) with or without 20 μM Pitstop 2. Mice were anesthetized throughout the experiment and kept warm by heating pads linked to thermoregulators (Harvard Apparatus Homeothermic Monitoring System Model 55-7020) that sense and maintain body temperature. After perfusion, the perfused section, as well as an adjacent proximal unperfused section of the ileum, were collected and processed for electron tomography. Tomograms were scored in a blinded fashion, except for tomograms from Dynasore treated samples, which were not blinded.

Downloaded from <http://science.sciencemag.org/> on May 13, 2020

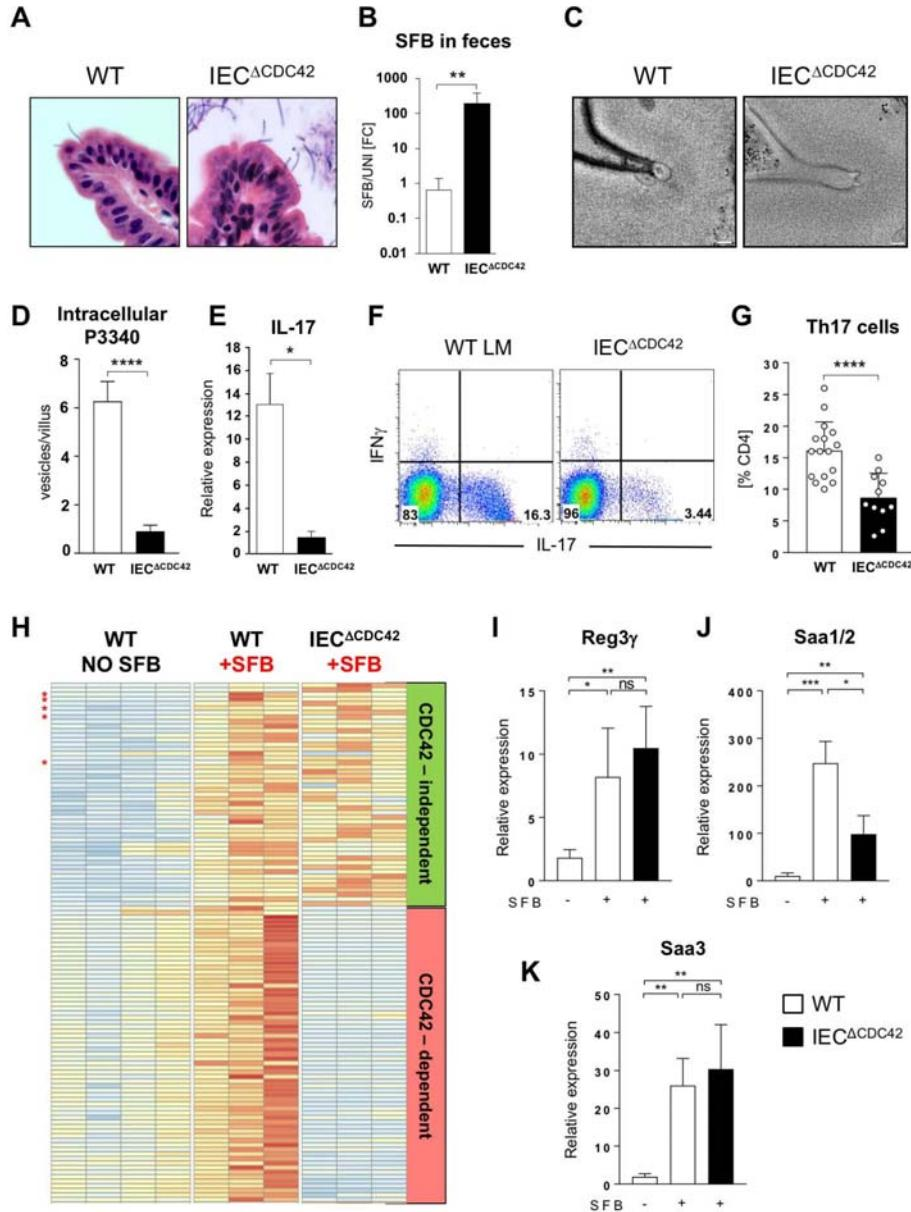


Fig. 7. Epithelial CDC42 is required for MATE, SFB antigen acquisition, and Th17 cell induction by SFB. (A) Hematoxylin and eosin staining of sections from terminal ileum of WT and IEC^{ΔCDC42} mice. SFB attachment on the surface of the villi is evident in both groups. (B) SFB levels in feces from WT and IEC^{ΔCDC42} mice. (C) MATE vesicles in SFB-IEC synapses in terminal ileum of WT and IEC^{ΔCDC42} mice. (D) Decrease in acquisition of P3340 by IEC in terminal ileum of IEC^{ΔCDC42} mice. (E) Decrease in IL-17 mRNA in terminal ileum of SFB-colonized IEC^{ΔCDC42} mice. (F and G) Decrease in small intestinal lamina propria (LP) Th17 cells in IEC^{ΔCDC42} mice. Plots in (F) were gated on TCR γ CD4 $^+$ lymphocytes. (G) Combined data from several independent experiments. (H) Relative expression levels of SFB-induced genes in IECs from WT and IEC^{ΔCDC42} mice. Only genes induced by SFB are depicted. Red stars indicate Saa1, Saa2, Saa3, Nos2, and Reg3g. Complete list of gene names is included in fig. S9. (I to K) Reverse transcription PCR (RT-PCR) for SFB-controlled genes on RNA isolated from IECs from WT and IEC^{ΔCDC42} mice as described in the materials and methods. Statistics, unpaired t test. * P < 0.05, ** P < 0.01, *** P < 0.005, **** P < 0.0001. Scale bars, (C) 100 nm.

Tamoxifen treatment for conditional deletion of CDC42

For conditional deletion, IEC^{ΔCDC42-CKO} mice and F/F, Non littermate controls were treated with tamoxifen by intraperitoneal injection. Each animal received two injections of 3 mg tamoxifen on Day 0 and Day 2. Mice were colonized with SFB on Day 5 and 5×10^5 MACS purified CD45.1 $^+$ 7B8 Tg T cells were transferred on Day 7 as described below. CD4 T cell proliferation and differentiation were examined on Day 11.

Lamina propria lymphocytes and CD4 T cell isolation and adoptive transfers

Lamina propria (LP) lymphocyte isolation and intracellular cytokine staining for IL-17 and ROR γ were performed as previously described (11). For adoptive transfers, CD45.1 CD4 T cells were purified to 95 to 98% purity from spleens and lymph nodes of SFB-negative 7B8 Tg mice (14) using anti-CD4 magnetic microbeads and MACS columns (Miltenyi Biotech). Purified 7B8 CD4 T cells were labeled with CellTrace Violet (CTV) Proliferation dye (Invitrogen C34557) as per manufacturer protocol. 0.5×10^6 to 1×10^6 labeled CD4 T cells were transferred intravenously into SFB-colonized CD45.2 recipient animals. Proliferation of transferred CD45.1 CD4 T cells was assessed 4 days later in mesenteric lymph nodes (MLNs) or spleen by CTV dye dilution.

Activated CDC42 assay and CDC42EP1 protein quantification

Mice colonized with SFB for 10 days and their noncolonized controls were sacrificed (5 mice for each condition) and intestinal epithelial cells isolated by scraping of distal ileum sections with glass slides and sonicated immediately in cold lysis buffer containing 0.05% NP-40. One milligram of lysate of each sample was incubated with 20 μg of GST-Human PAK1-PBD and glutathione agarose beads for one hour (Cell Signaling #8819). GTP-bound CDC42 was precipitated and resolved on a 10% SDS-PAGE gel and transferred to a nitrocellulose membrane

at 300 mA for 1 hour. Membranes were blocked with 5% milk and probed with antibodies against CDC42 (1:1000, Abcam, ab65433) to reveal active and total CDC42. Total levels of CDC42EP1 (1:1000, Abcam, ab135331), and beta actin (1:1000, Santa Cruz, sc4778) were also analyzed by means of Western blot. Anti-rabbit or anti-mouse secondary antibodies conjugated with HRP were used for visualization.

RNA-sequencing and analysis

For RNA-sequencing (RNA-seq), SFB-negative wild-type (WT) and IEC^{ΔCDC42} mice were colonized with SFB by oral gavage. A single litter of eight 11-week old animals was used for the

experiment. KO animals were all F/F, Vil-Cre and WT controls included F/F, Non; F/+;Non and F/+;Vil-Cre genotypes. In addition, two female Jackson B6 mice of similar age were co-housed and included in the WT No SFB group. 3 weeks after SFB gavage, IECs were collected from terminal ileum of individual animals by scraping with a glass slide, immediately placed in 1 ml of cold Trizol and homogenized by passing through a syringe needle and vortexing. RNA was isolated as per the manufacturer protocol and sent for RNA-seq. RNA-seq was performed at the JP Sulzberger Columbia Genome Center. Poly-A pull-down was performed to enrich mRNAs from total RNA

samples, followed by library construction using Illumina TruSeq chemistry. Libraries were then sequenced using Illumina NovaSeq 6000. RTA (Illumina) was used for base calling and bcl2fastq2 (version 2.20) for converting BCL to fastq format, coupled with adaptor trimming. Pseudoalignment was performed to a kallisto index created from transcriptomes (Mouse: GRCm38) using kallisto (0.44.0). Differential gene expression analysis was performed using DESeq2. For the differential analysis, trimming was performed using the following steps. First, genes that were not significantly changed between WT and WT + SFB groups were excluded ($p_{adj} < 0.05$). Next, genes with very low expression level (transcripts per million, tpm < 5 in at least 9 out of the 10 samples) were also excluded. An unusually high level of Ig gene transcripts was observed in a few samples and, therefore, Ig genes were excluded from the analysis. Finally, two of the three groups contained male animals and, therefore, Y-chromosome genes were also excluded. The remaining genes were grouped as described on the legends of fig. S9 and S10.

Quantitative PCR

Total mRNA was isolated from 0.5 cm pieces of terminal ileum using Trizol and cDNA prepared using SuperScript III First Strand Synthesis System (Invitrogen). Q-PCR was performed on LightCycler 480 (Roche) using the following primers:

Rpl37 (FWD 5'-CCTACCACCTTCAGAACGTC-GAC-3', REV 5'-CTTTAGGTGCCTCATCCGACCA-3')

Rpl38 (FWD 5'-AGGATGCCAAGTCTGTCA-AGA-3', REV 5'-TCCTTGCTGTGATAACCAG-GG-3')

Il17a (FWD 5'-GGACTCTCACCGCAATGA-3', REV 5'-GGCACTGAGCTTCCCAGATC-3')

Saa1/2 (FWD 5'-GTAATTGGGGTCTTTGCC-3', REV 5'-TTCTGCTCCCTGCTCCTG-3')

Saa3 (FWD 5'-CCGAGCACGAGCAGGAT-3', REV 5'-CCAGGATCAAGATGAAAGAATG-3')

Reg3γ (FWD 5'-CCTGATGCTCTTCTCA-GG-3', REV 5'-ATGTCCTGAGGGCCTCTTT-3').

Relative expression was calculated by the $\Delta\Delta Ct$ method based on normalization to the house keeping genes *Rpl37* or *Rpl38*.

REFERENCES AND NOTES

- L. V. Hooper, A. J. Macpherson, Immune adaptations that maintain homeostasis with the intestinal microbiota. *Nat. Rev. Immunol.* **10**, 159–169 (2010). doi: [10.1038/nri2710](https://doi.org/10.1038/nri2710); pmid: [20182457](https://pubmed.ncbi.nlm.nih.gov/20182457/)
- Y. Furusawa et al., Commensal microbe-derived butyrate induces the differentiation of colonic regulatory T cells. *Nature* **504**, 446–450 (2013). doi: [10.1038/nature12721](https://doi.org/10.1038/nature12721); pmid: [24226770](https://pubmed.ncbi.nlm.nih.gov/24226770/)
- P. M. Smith et al., The microbial metabolites, short-chain fatty acids, regulate colonic Treg cell homeostasis. *Science* **341**, 569–573 (2013). doi: [10.1126/science.1241165](https://doi.org/10.1126/science.1241165); pmid: [23828891](https://pubmed.ncbi.nlm.nih.gov/23828891/)
- N. Arpaia et al., Metabolites produced by commensal bacteria promote peripheral regulatory T-cell generation. *Nature* **504**, 451–455 (2013). doi: [10.1038/nature12726](https://doi.org/10.1038/nature12726); pmid: [24226773](https://pubmed.ncbi.nlm.nih.gov/24226773/)
- Y. Shen et al., Outer membrane vesicles of a human commensal mediate immune regulation and disease protection. *Cell Host Microbe* **12**, 509–520 (2012). doi: [10.1016/j.chom.2012.08.004](https://doi.org/10.1016/j.chom.2012.08.004); pmid: [23000000](https://pubmed.ncbi.nlm.nih.gov/23000000/)

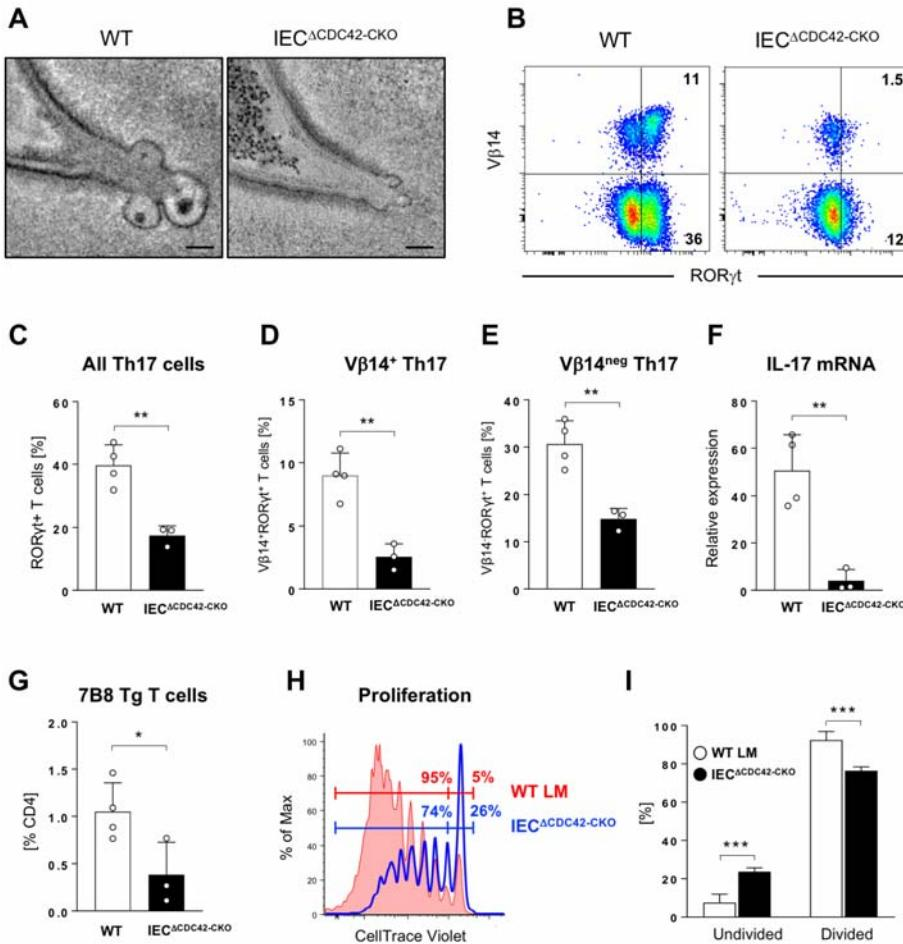


Fig. 8. Epithelial CDC42 is required for activation of SFB-specific CD4 T cells and induction of SFB-specific Th17 cells. WT and IEC^{ΔCDC42-CKO} mice were treated with tamoxifen before SFB colonization and transfer of naïve P3340-specific 7B8 Tg CD4 T cells (Materials and methods). (A) MATE vesicles in SFB-IEC synapses in terminal ileum of tamoxifen-treated WT and IEC^{ΔCDC42-CKO} mice. (B to E) Decrease in endogenous SI LP Th17 cells in tamoxifen-treated IEC^{ΔCDC42-CKO} mice 6 days after SFB colonization. (B) Representative fluorescence-activated cell sorting plots of LP lymphocytes gated on TCR⁺CD4⁺ cells. [(C) to (E)] Statistic based on the gating in (B). (F) Decrease in IL-17 mRNA in terminal ileum of tamoxifen-treated IEC^{ΔCDC42-CKO} mice. (G) Decreased expansion of adoptively transferred P3340-specific 7B8 Tg CD4 T cells in MLNs of tamoxifen-treated IEC^{ΔCDC42-CKO} mice 4 days after transfer. (H and I) Proliferation of 7B8 Tg CD4 T cells in MLN of tamoxifen-treated WT littermate (WT LM) or IEC^{ΔCDC42-CKO} recipient mice on day 4 after adoptive transfer. One of three independent experiments with similar results. Error bars, standard deviation. Statistics, unpaired two-tailed *t* test. **P* < 0.05, ***P* < 0.01, ****P* < 0.005, *****P* < 0.001. Scale bars, (A) 100 nm.

6. H. Chu et al., Gene-microbiota interactions contribute to the pathogenesis of inflammatory bowel disease. *Science* **352**, 1116–1120 (2016). doi: [10.1126/science.aad9948](https://doi.org/10.1126/science.aad9948); pmid: [27230380](https://pubmed.ncbi.nlm.nih.gov/27230380/)
7. H. L. Klaasen et al., Intestinal, segmented, filamentous bacteria in a wide range of vertebrate species. *Lab. Anim.* **27**, 141–150 (1993). doi: [10.1258/002367793793801041](https://doi.org/10.1258/002367793793801041); pmid: [8501895](https://pubmed.ncbi.nlm.nih.gov/8501895/)
8. G. L. Talham, H. Q. Jiang, N. A. Bos, J. J. Cebray, Segmented filamentous bacteria are potent stimuli of physiologically normal state of the murine gut mucosal immune system. *Infect. Immun.* **67**, 1992–2000 (1999). pmid: [10085047](https://pubmed.ncbi.nlm.nih.gov/10085047/)
9. A. Sczesnak et al., The genome of Th17 cell-inducing segmented filamentous bacteria reveals extensive auxotrophy and adaptations to the intestinal environment. *Cell Host Microbe* **10**, 260–272 (2011). doi: [10.1016/j.chom.2011.08.005](https://doi.org/10.1016/j.chom.2011.08.005); pmid: [21925113](https://pubmed.ncbi.nlm.nih.gov/21925113/)
10. T. Prakash et al., Complete genome sequences of rat and mouse segmented filamentous bacteria, a potent inducer of Th17 cell differentiation. *Cell Host Microbe* **10**, 273–284 (2011). doi: [10.1016/j.chom.2011.08.007](https://doi.org/10.1016/j.chom.2011.08.007); pmid: [21925114](https://pubmed.ncbi.nlm.nih.gov/21925114/)
11. I. I. Ivanov et al., Induction of intestinal Th17 cells by segmented filamentous bacteria. *Cell* **139**, 485–498 (2009). doi: [10.1016/j.cell.2009.09.033](https://doi.org/10.1016/j.cell.2009.09.033); pmid: [19836068](https://pubmed.ncbi.nlm.nih.gov/19836068/)
12. V. Gaboriau-Routhiau et al., The key role of segmented filamentous bacteria in the coordinated maturation of gut helper T cell responses. *Immunity* **31**, 677–689 (2009). doi: [10.1016/j.jimmuni.2009.08.020](https://doi.org/10.1016/j.jimmuni.2009.08.020); pmid: [19833089](https://pubmed.ncbi.nlm.nih.gov/19833089/)
13. Y. Goto et al., Segmented filamentous bacteria antigens presented by intestinal dendritic cells drive mucosal Th17 cell differentiation. *Immunity* **40**, 594–607 (2014). doi: [10.1016/j.jimmuni.2014.03.005](https://doi.org/10.1016/j.jimmuni.2014.03.005); pmid: [24684957](https://pubmed.ncbi.nlm.nih.gov/24684957/)
14. Y. Yang et al., Focused specificity of intestinal TH17 cells towards commensal bacterial antigens. *Nature* **510**, 152–156 (2014). doi: [10.1038/nature13279](https://doi.org/10.1038/nature13279); pmid: [24739972](https://pubmed.ncbi.nlm.nih.gov/24739972/)
15. I. I. Ivanov et al., Specific microbiota direct the differentiation of IL-17-producing T-helper cells in the mucosa of the small intestine. *Cell Host Microbe* **4**, 337–349 (2008). doi: [10.1016/j.chom.2008.09.009](https://doi.org/10.1016/j.chom.2008.09.009); pmid: [18854238](https://pubmed.ncbi.nlm.nih.gov/18854238/)
16. A. M. Farkas et al., Induction of Th17 cells by segmented filamentous bacteria in the murine intestine. *J. Immunol. Methods* **421**, 104–111 (2015). doi: [10.1016/j.jim.2015.03.020](https://doi.org/10.1016/j.jim.2015.03.020); pmid: [25858227](https://pubmed.ncbi.nlm.nih.gov/25858227/)
17. C. P. Davis, D. C. Savage, Habitat, succession, attachment, and morphology of segmented, filamentous microbes indigenous to the murine gastrointestinal tract. *Infect. Immun.* **10**, 948–956 (1974). pmid: [426712](https://pubmed.ncbi.nlm.nih.gov/426712/)
18. J. E. Snellen, D. C. Savage, Freeze-fracture study of the filamentous, segmented microorganism attached to the murine small bowel. *J. Bacteriol.* **134**, 1099–1107 (1978). pmid: [659364](https://pubmed.ncbi.nlm.nih.gov/659364/)
19. K. Atarashi et al., Th17 cell induction by adhesion of microbes to intestinal epithelial cells. *Cell* **163**, 367–380 (2015). doi: [10.1016/j.cell.2015.08.058](https://doi.org/10.1016/j.cell.2015.08.058); pmid: [26411289](https://pubmed.ncbi.nlm.nih.gov/26411289/)
20. K. E. Yamauchi, J. Snel, Transmission electron microscopic demonstration of phagocytosis and intracellular processing of segmented filamentous bacteria by intestinal epithelial cells of the chick ileum. *Infect. Immun.* **68**, 6496–6504 (2000). doi: [10.1128/IAI.68.11.6496-6504.2000](https://doi.org/10.1128/IAI.68.11.6496-6504.2000); pmid: [11035767](https://pubmed.ncbi.nlm.nih.gov/11035767/)
21. M. Caselli, J. Holton, P. Boldrini, D. Vaira, G. Calò, Morphology of segmented filamentous bacteria and their patterns of contact with the follicle-associated epithelium of the mouse terminal ileum: Implications for the relationship with the immune system. *Gut Microbes* **1**, 367–372 (2010). doi: [10.4161/gmic.16.14390](https://doi.org/10.4161/gmic.16.14390); pmid: [21468217](https://pubmed.ncbi.nlm.nih.gov/21468217/)
22. T. G. Tan et al., Identifying species of symbiont bacteria from the human gut that, alone, can induce intestinal Th17 cells in mice. *Proc. Natl. Acad. Sci. U.S.A.* **113**, E8141–E8150 (2016). doi: [10.1073/pnas.1617460113](https://doi.org/10.1073/pnas.1617460113); pmid: [27911839](https://pubmed.ncbi.nlm.nih.gov/27911839/)
23. M. A. Jepson, M. A. Clark, N. L. Simmons, B. H. Hirst, Actin accumulation at sites of attachment of indigenous apathogenic segmented filamentous bacteria to mouse ileal epithelial cells. *Infect. Immun.* **61**, 4001–4004 (1993). pmid: [8359925](https://pubmed.ncbi.nlm.nih.gov/8359925/)
24. S. Mayor, R. E. Pagano, Pathways of clathrin-independent endocytosis. *Nat. Rev. Mol. Cell Biol.* **8**, 603–612 (2007). doi: [10.1038/nrm2216](https://doi.org/10.1038/nrm2216); pmid: [17609668](https://pubmed.ncbi.nlm.nih.gov/17609668/)
25. R. Sakamori et al., Cdc42 and Rab8a are critical for intestinal stem cell division, survival, and differentiation in mice. *J. Clin. Invest.* **122**, 1052–1065 (2012). doi: [10.1172/JCI60282](https://doi.org/10.1172/JCI60282); pmid: [22354172](https://pubmed.ncbi.nlm.nih.gov/22354172/)
26. C. Panea et al., Intestinal monocyte-derived macrophages control commensal-specific Th17 responses. *Cell Reports* **12**, 1314–1324 (2015). doi: [10.1016/j.celrep.2015.07.040](https://doi.org/10.1016/j.celrep.2015.07.040); pmid: [26279572](https://pubmed.ncbi.nlm.nih.gov/26279572/)
27. D. Geem et al., Specific microbiota-induced intestinal Th17 differentiation requires MHC class II but not GALT and mesenteric lymph nodes. *J. Immunol.* **193**, 431–438 (2014). doi: [10.4049/jimmunol.1303167](https://doi.org/10.4049/jimmunol.1303167); pmid: [24899505](https://pubmed.ncbi.nlm.nih.gov/24899505/)
28. D. G. Chase, S. L. Erlandsen, Evidence for a complex life cycle and endospore formation in the attached, filamentous, segmented bacterium from murine ileum. *J. Bacteriol.* **127**, 572–583 (1976). pmid: [931952](https://pubmed.ncbi.nlm.nih.gov/931952/)
29. L. C. Yu et al., Enteric dysbiosis promotes antibiotic-resistant bacterial infection: Systemic dissemination of resistant and commensal bacteria through epithelial transcytosis. *Am. J. Physiol. Gastrointest. Liver Physiol.* **307**, G824–G835 (2014). doi: [10.1152/ajpgi.00070.2014](https://doi.org/10.1152/ajpgi.00070.2014); pmid: [25059827](https://pubmed.ncbi.nlm.nih.gov/25059827/)
30. R. J. Cummings et al., Different tissue phagocytes sample apoptotic cells to direct distinct homeostasis programs. *Nature* **539**, 565–569 (2016). doi: [10.1038/nature20183](https://doi.org/10.1038/nature20183); pmid: [27828940](https://pubmed.ncbi.nlm.nih.gov/27828940/)
31. T. Feng, C. O. Elson, Adaptive immunity in the host-microbiota dialog. *Mucosal Immunol.* **4**, 15–21 (2011). doi: [10.1038/mi.2010.60](https://doi.org/10.1038/mi.2010.60); pmid: [20944557](https://pubmed.ncbi.nlm.nih.gov/20944557/)
32. J. N. Choi et al., *Helicobacter* species are potent drivers of colonic T cell responses in homeostasis and inflammation. *Sci. Immunol.* **2**, eaal5068 (2017). doi: [10.1126/sciimmunol.aal5068](https://doi.org/10.1126/sciimmunol.aal5068); pmid: [28733471](https://pubmed.ncbi.nlm.nih.gov/28733471/)
33. M. Xu et al., c-MAF-dependent regulatory T cells mediate immunological tolerance to a gut pathobiont. *Nature* **554**, 373–377 (2018). doi: [10.1038/nature25500](https://doi.org/10.1038/nature25500); pmid: [29414937](https://pubmed.ncbi.nlm.nih.gov/29414937/)
34. L. Yang et al., Rho GTPase Cdc42 coordinates hematopoietic stem cell quiescence and niche interaction in the bone marrow. *Proc. Natl. Acad. Sci. U.S.A.* **104**, 5091–5096 (2007). doi: [10.1073/pnas.0610819104](https://doi.org/10.1073/pnas.0610819104); pmid: [17360364](https://pubmed.ncbi.nlm.nih.gov/17360364/)
35. F. el Marjou et al., Tissue-specific and inducible Cre-mediated recombination in the gut epithelium. *Genesis* **39**, 186–193 (2004). doi: [10.1002/gene.20042](https://doi.org/10.1002/gene.20042); pmid: [15282745](https://pubmed.ncbi.nlm.nih.gov/15282745/)
36. D. N. Mastronarde, Automated electron microscope tomography using robust prediction of specimen movements. *J. Struct. Biol.* **152**, 36–51 (2005). doi: [10.1016/j.jsb.2005.07.007](https://doi.org/10.1016/j.jsb.2005.07.007); pmid: [16182563](https://pubmed.ncbi.nlm.nih.gov/16182563/)
37. J. R. Kremer, D. N. Mastronarde, J. R. McIntosh, Computer visualization of three-dimensional image data using IMOD. *J. Struct. Biol.* **116**, 71–76 (1996). doi: [10.1006/jsb.1996.0013](https://doi.org/10.1006/jsb.1996.0013); pmid: [8742726](https://pubmed.ncbi.nlm.nih.gov/8742726/)
38. D. N. Mastronarde, Correction for non-perpendicularity of beam and tilt axis in tomographic reconstructions with the IMOD package. *J. Microsc.* **230**, 212–217 (2008). doi: [10.1111/j.1365-2818.2008.01977.x](https://doi.org/10.1111/j.1365-2818.2008.01977.x); pmid: [18445149](https://pubmed.ncbi.nlm.nih.gov/18445149/)
39. V. F. Shih et al., Homeostatic IL-23 receptor signaling limits Th17 response through IL-22-mediated containment of commensal microbiota. *Proc. Natl. Acad. Sci. U.S.A.* **111**, 13942–13947 (2014). doi: [10.1073/pnas.1323852111](https://doi.org/10.1073/pnas.1323852111); pmid: [25201978](https://pubmed.ncbi.nlm.nih.gov/25201978/)
40. L. Jiang, H. Lawsky, R. M. Coloso, M. A. Dudley, R. P. Ferraris, Intestinal perfusion induces rapid activation of immediate-early genes in weaning rats. *Am. J. Physiol. Regul. Integr. Comp. Physiol.* **281**, R1274–R1282 (2001). doi: [10.1152/ajpregu.2001.281.4.R1274](https://doi.org/10.1152/ajpregu.2001.281.4.R1274); pmid: [11557636](https://pubmed.ncbi.nlm.nih.gov/11557636/)

ACKNOWLEDGMENTS

We thank D. Littman (NYU) for generously providing 7B8 Tg mice and anti-P3340 antibody. We thank Y. Zheng (Cincinnati Children's Hospital) for providing CDC42-flox mice. We thank C. Jobin (University of Florida) for providing AIEC strain LF82. We thank E. Byington from the JP Sulzberger Columbia Genome Center for help with RNA-seq analysis. We thank members of the Ivanov and Gao laboratories for technical help. We thank S. Ghosh and S. Reiner for providing advice and feedback throughout the project and for help with the manuscript. We thank E. Reeder from LNInnovations and M. Murphy for assistance with illustrations.

Funding: This work was supported by funding from the following sources: NIH R21 AI126305 and R01 DK098378 (I.I.I.); P50 GM082545 (P.J.B.); NIH R01 DK102934 and ACS Research Scholar Award 15-060-01-TBE (N.G.); NSF/BIO/IOS 1456673 (R.P.F.); NIH R01 AI0120243 (N.G. and R.P.F.); AMED-LEAP JP17 g0010003 and Takeda Science Foundation (K.H.); CIHR Grant 324932 (B.K.C.); Columbia University Schaefer Research Award (I.I.I.); and Pew Charitable Trust Innovation Fund Award 00031379 (I.I.I. and P.J.B.).

Author contributions: P.J.B and I.I.I. conceived and supervised the study. M.S.L., L.P.A. and I.I.I. designed the study, experiments, and wrote the manuscript. M.S.L. performed all electron tomography and electron microscopy experiments. L.P.A. performed in vivo experiments and analyzed the data. X.Z., J.V., M.G.-D., S.S., C.L., K.I., E.Y.P., S.N., S.B., W.E., B.K.C., R.P.F., K.H., I.D.I., and N.G. participated in performing experiments, provided intellectual expertise, and helped to interpret experimental results. X.Z. and N.G. performed CDC42 activation assays and confocal microscopy experiments and analysis. J.V. performed externalized intestinal loops experiments. M.G.-D., L.P.A., and K.I. performed analysis of intestinal immune subsets in IEC^{ΔCDC42} and IEC^{ΔCDC42-OKO} mice and analyzed the data. S.S. performed confocal microscopy experiments and analysis. C.L. prepared samples for RNA-seq and performed RT-PCR experiments. E.Y.P. analyzed electron tomography data. S.N. and K.H. performed gnotobiotic experiments. M.N. isolated and provided *B. adolescentis*. W.E. and B.K.C. performed colonization experiments with AIEC strain NRG857c. I.D.I. helped with analysis of RNA-seq data and prepared corresponding figures. **Competing interests:** K.H. is a scientific advisory board member at Vedanta Biosciences. **Data and materials availability:** The accession number for the RNA-seq datasets is NCBI BioProject GSE124848. All other data needed to evaluate the conclusions in this paper are present either in the main text or the supplementary materials.

SUPPLEMENTARY MATERIALS

www.sciencemag.org/content/363/6431/eaat4042/suppl/DC1
Figs. S1 to S12
Movies S1 and S2

22 February 2018; resubmitted 11 October 2018
Accepted 28 January 2019
10.1126/science.eaat4042

Endocytosis of commensal antigens by intestinal epithelial cells regulates mucosal T cell homeostasis

Mark S. Ladinsky, Leandro P. Araujo, Xiao Zhang, John Veltri, Marta Galan-Diez, Salima Soualhi, Carolyn Lee, Koichiro Irie, Elisha Y. Pinker, Seiko Narushima, Sheila Bandyopadhyay, Manabu Nagayama, Wael Elhenawy, Brian K. Coombes, Ronaldo P. Ferraris, Kenya Honda, Iliyan D. Iliev, Nan Gao, Pamela J. Bjorkman and Ivaylo I. Ivanov

Science 363 (6431), eaat4042.
DOI: 10.1126/science.aat4042

Hooking into antigen transfer

Segmented filamentous bacteria (SFB) are anaerobic, spore-forming, clostridia-like organisms that are important immune modulators in the mammalian gut. For some reason, SFB do not provoke inflammatory responses. Ladinsky *et al.* probed the mechanistic basis of this soothing effect in mice. SFB attach tightly to intestinal epithelial cells via a hook-like structure. Bacterial material is extruded from the hook and enters the host cell by endocytosis. An extruded SFB protein called P3340 is shuttled by the host protein cell division control protein 42 homolog (CDC42) through the endosomelysosome vesicular pathway to the basolateral side of the intestinal epithelial cell. Here, it prompts an immunomodulatory SFB-specific CD4 T helper 17 cell response, possibly via intestinal macrophages.

Science, this issue p. eaat4042

ARTICLE TOOLS

<http://science.sciencemag.org/content/363/6431/eaat4042>

SUPPLEMENTARY MATERIALS

<http://science.sciencemag.org/content/suppl/2019/03/06/363.6431.eaat4042.DC1>

RELATED CONTENT

<http://stm.sciencemag.org/content/scitransmed/5/193/193ra91.full>
<http://stm.sciencemag.org/content/scitransmed/6/220/220ra11.full>
<http://stm.sciencemag.org/content/scitransmed/4/118/118ra12.full>
<http://stm.sciencemag.org/content/scitransmed/6/225/225ra28.full>

REFERENCES

This article cites 40 articles, 13 of which you can access for free
<http://science.sciencemag.org/content/363/6431/eaat4042#BIBL>

PERMISSIONS

<http://www.sciencemag.org/help/reprints-and-permissions>

Use of this article is subject to the [Terms of Service](#)

Science (print ISSN 0036-8075; online ISSN 1095-9203) is published by the American Association for the Advancement of Science, 1200 New York Avenue NW, Washington, DC 20005. The title *Science* is a registered trademark of AAAS.

Copyright © 2019 The Authors, some rights reserved; exclusive licensee American Association for the Advancement of Science. No claim to original U.S. Government Works